Journal of Catalysis 276 (2010) 371–381

Contents lists available at ScienceDirect

Journal of Catalysis

journal homepage: www.elsevier.com/locate/jcat

Selective oxidation of ammonia on RuO_2(1 1 0): A combined DFT and KMC study

Sampyo Hong [a], Altaf Karim [b], Talat S. Rahman [a,*], Karl Jacobi [c], Gerhard Ertl [c]

[a] Department of Physics, University of Central Florida, Orlando, FL 32816-2385, United States
[b] Center for Functional Nanomaterials, Brookhaven National Laboratory, Upton, NY 11973-5000, United States
[c] Department of Physical Chemistry, Fritz-Haber-Institut der Max-Planck-Gesellschaft, Faradayweg 4–6, D-14195 Berlin, Germany

ARTICLE INFO

Article history:
Received 19 July 2010
Revised 20 September 2010
Accepted 29 September 2010
Available online 2 November 2010

Keywords:
Ruthenium
Oxide
Ammonia
Oxidation
Kinetic Monte Carlo
Density functional theory
Catalysis
Selectivity

ABSTRACT

We have used a combination of density functional theory (DFT) and kinetic Monte Carlo (KMC) simulations to calculate the reaction rates for the selective oxidation of ammonia on RuO_2(1 1 0). Our KMC simulations of 18 reactions among $NH_{x(x=0-3)}$ and $OH_{x(x=0-2)}$ species on RuO_2(1 1 0) show 93% selectivity for NO, in close agreement with experiment (~95%). The chief factor in the high selectivity for NO on the RuO_2(1 1 0) surface is the significantly reduced N diffusion (via N blocking) caused by various intermediates present on the RuO_2(1 1 0) surface, which severely inhibits the recombination rate of N + N → N_2 but interfere far less with that of N + O → NO owing to the nearby availability of O from dissociation of O_2.

1. Introduction

Catalytic oxidation of ammonia is of much industrial importance for two reasons. Through the so-called Ostwald process, it leads to the formation of nitric oxide. Alternatively, it can yield nitrogen and water, freeing waste streams of ammonia. In the choice of a catalyst for ammonia oxidation, selectivity for the product becomes as important, if not more so, as reactivity of the process. In this regard, recent work by Wang et al. [1] has shown the RuO_2(1 1 0) surface to be particularly appealing. This proposition is not surprising in light of the seminal work by Over et al. [2] that at high temperature a RuO_2(1 1 0) film several nanometers thick formed from O_2 dosing of Ru(0 0 0 1) is much more reactive than the pristine metal surfaces for such processes as CO oxidation. Since then a body of experimental work [3–6] has focused on establishing the reactivity of the interestingly structured RuO_2(1 1 0) surface, whose stoichiometry is depicted in Fig. 1. What makes RuO_2(1 1 0) surface a good candidate for facilitation of chemical reactions is the presence of two types of atoms with unsaturated bonds along the [0 0 1] direction: the twofold coordinated oxygen atom (O-bridge) and the fivefold coordinated Ru atom (Ru-cus), both of which form linear arrays. The latter in particular is the adsorption site for a number of atomic and molecular species, including ammonia [1]. Both O-bridge (O_{br}) and Ru-cus sites (Ru_{cus}) can facilitate chemical reactions, as has been seen in the case of CO oxidation on this surface [7]. For ammonia oxidation, however, the salient role is played by the rows of Ru_{cus} atoms on this surface, as noted in both experiments [1] and theoretical calculations [8,9].

According to recent experiments O_{br} atoms in RuO_2 (1 1 0) are mostly inactive during the reaction, and ammonia decomposition reactions occur mainly between reactants adsorbed side-by-side at the Ru_{cus} sites, which run parallel to the row of O_{br} atoms, indicating that the RuO_2(1 1 0) surface effectively acts a one-dimensional (1D) chain catalyst aligned along the [0 0 1] direction [1]. In fact, ammonia undergoes no reaction on the stoichiometric RuO_2(1 1 0) surface other than simple adsorption and desorption on the Ru_{cus} sites: only when oxygen atoms occupy the Ru_{cus} sites (let us label these O_{cus}), as O_2 dissociates on RuO_2(1 1 0), does that surface promote the decomposition and subsequent oxidation of ammonia. The first-stage NH_3 decomposition (to NH_2) occurs around 90 K; successive annealing to 250 K (to 300 K in Ref. [9]) produces N. High reactivity of the surface, however, occurs at a higher temperature (around 530 K) because of the high desorption temperature for NO. At low temperatures NO-formation is poisoned by surface water molecules, which desorb around 400 K [1,9].

The reactivity of RuO_2(1 1 0) for ammonia oxidation already makes it a strong contender to replace currently used Pt gauges in the Ostwald process. Contrary to UHV experiments, however, a

* Corresponding author. Fax: +1 407 823 5112.
E-mail address: talat@physics.ucf.edu (T.S. Rahman).

0021-9517/$ - see front matter © 2010 Elsevier Inc. All rights reserved.
doi:10.1016/j.jcat.2010.09.029

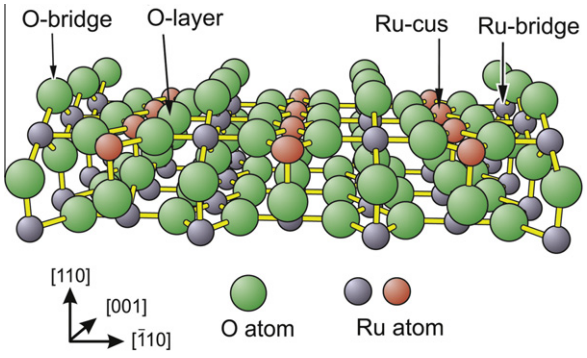

Fig. 1. Ball-and-stick model of the stoichiometric RuO_2(1 1 0) surface. Small and large balls represent Ru and O atoms, respectively.

recent experiment at ambient O_2 pressure indicates a reduced reactivity of the RuO_2(1 1 0) surface (toward CO oxidation) [10]. Thus, a so-called pressure-gap possibly exists. Nevertheless, what is most remarkable in terms of the reactivity of RuO_2(1 1 0) for ammonia oxidation in UHV condition is the selectivity of the end product. On the RuO_2(1 1 0) surface Wang et al., obtained almost perfect selectivity toward NO in UHV conditions at the reaction temperature of 500–530 K depending on O_2 pressure in the system [1]. At low O_2 pressure ($p[O_2]/p[NH_3] \leq 0.3$), N_2 is the dominant product; however, as the ratio of O_2 to NH_3 pressure increases to 0.3, NO becomes the dominant product; and as this ratio approaches 10, nearly 100% selectivity is obtained. Interestingly neither N_2O nor NO_2 was detected as product in the experiments [1,9].

Recently several works have been devoted to the theoretical study of the energetics and geometrical structures of $NH_{x(x=1-3)}$ on the RuO_2(1 1 0) surface using methods based on DFT [8,9]. These studies have confirmed that ammonia adsorbs (with N toward the surface) with a large adsorption energy (≈1.55 eV) and that the lone electron pair on the nitrogen atom is responsible for the strong bond to Ru_{cus}. Upon adsorption, NH_3 forms a hydrogen bond with O_{br} or with O_{cus}. O_{br} may, in principle, participate in H abstraction in the various stages of the ammonia oxidation reaction. However, it is the hydrogen bond with O_{cus} that weakens the strength of the N–H bond of ammonia. As a result, activation energy for ammonia decomposition can be relatively low (≤0.76 eV).

The DFT studies carried out so far have also been helpful in mapping out the energetics of various reaction paths. They do not, however, address the issue of selectivity for the RuO_2(1 1 0) surface, which appears to be capable of converting NH_3 to either NO or N_2, merely by controlling the oxygen pressure in the experimental chamber. The reason is that while *ab initio* electronic structure calculations provide a reliable way of determining the activation energy barriers and transition states of expected reactions, they cannot by themselves address the issues of reaction kinetics upon which selectivity depends. A suitable method for determining the latter is KMC simulations, which have recently been applied by a number of groups to examine relative rates of competing reactions on surfaces. An instructive example is the recent *ab initio* KMC study confirming and illuminating the high reactivity of CO oxidation reactions on RuO_2(1 1 0) [11]. Our aim in this work is likewise to use a combination of DFT and KMC simulations to examine the relative rates of ammonia oxidation reactions on RuO_2(1 1 0). We are interested in identifying competing reactions, isolating the rate-limiting processes, and obtaining measures of reactivity of the surface and conditions for selectivity in the products for the specific system of interest. The results reported in this study are a completion of our preliminary study, whose results have been made public [12]. Section 2 summarizes our theoretical methods. Section 3 describes and analyzes our results. Section 4 summaries our conclusions.

2. Theoretical methods

2.1. Model system

We present a stick-and-ball model for the stoichiometric RuO_2(1 1 0) surface in Fig. 1. In the bulk, the coordination of Ru atoms is six while that of the O atoms is three. The RuO_2(1 1 0) surface, however, is remarkable in that it exposes rows of undercoordinated Ru [Ru-cus in Fig. 1] and O atoms [O-bridge in Fig. 1], both of which have unpaired bonds along the surface normal. Shown in Fig. 1 are also the Ru-bridge and O-layer atoms, which are fully coordinated. As has been shown, Ru_{cus} is the most active site on this surface, though O_{br} also participates in some reactions. The model system consists also of oxygen molecules that are found to dissociatively adsorb on RuO_2(1 1 0) surface [13], the O atoms occupying the Ru_{cus} sites. The model system would be incomplete without such intermediates as NH_2, NH, N, OH, and H_2O on RuO_2(1 1 0) (see Fig. 2).

2.2. Calculations of the total energy

To calculate the geometry and energetics for the catalytic ammonia decomposition reactions on the RuO_2(1 1 0) surface, we have carried out DFT calculations [14] of the total energy using a plane wave basis set, in the ultrasoft pseudopotential scheme [15]. Our pseudopotential for Ru includes 4d, 5s and 5p states as the valence states with a scalar-relativistic correction while those for H, N and O include 1s (in case of H) or 2s and 2p states (in case of N and O) as the valence states [16]. For exchange–correlation energy, we used the Perdew–Burke–Ernzerhof (PBE) functional [17].

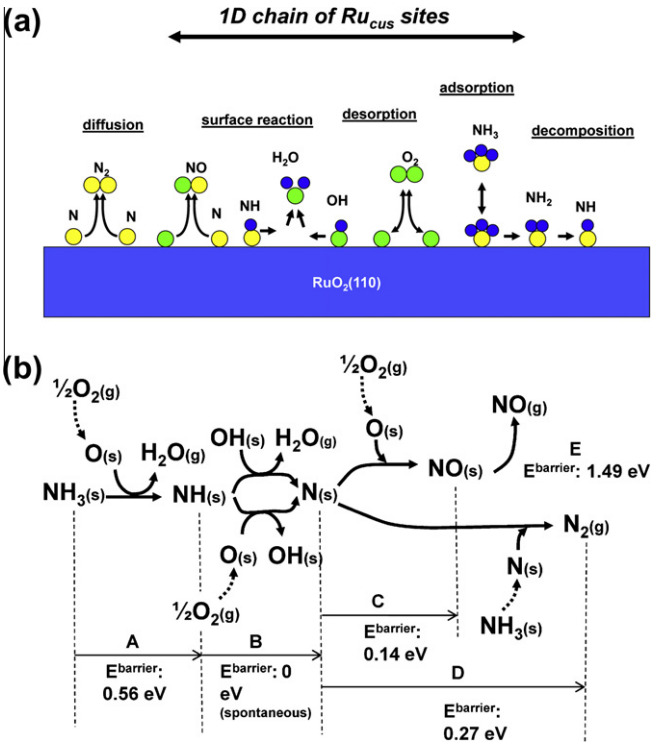

Fig. 2. (a) Various elementary processes (adsorption, desorption, decomposition, diffusion, and surface reactions) involving the intermediates considered in our simulations. (b) A possible scenario for the different stages in the ammonia decomposition process on RuO_2(1 1 0).

Table 1
Calculated structures of pertinent free molecules.

	d(N–X) X = H,N,O		θ(X–N–X) X = H,O	
	This study (Å)	Experiment (Å)	This study	Experiment
NH_3	1.023	1.017	106.1°	107.8°
N_2O	1.142 (N–N)	1.126	–	–
	1.197 (N–O)	1.186		
NO_2	1.211	1.197	133.8°	134.3°
N_2	1.109	1.112	–	–
NO	1.116	1.115	–	–

We used a kinetic energy cutoff of 408 eV for the plane wave basis set. The computer code was Quantum Espresso [18]. To check transferability of our pseudopotentials, we calculated the structures of various free molecules including NH_3, N_2 and NO (see Table 1), which are in good agreement with experiment.

The Monkhorst–Pack scheme was used for k-point sampling in the Brillouin zone using a $(3 \times 6 \times 1)$ grid, which resulted in eight irreducible k-points [19]. We used a Fermi level smearing of 0.19 eV [20]. For relaxation of the electronic degrees of freedom, we used Davidson iterative diagonalization with overlap matrix while for the ionic relaxations we used a BFGS quasi-Newton algorithm. The convergence threshold for relaxation of the electronic degree of freedom was set to 1.36×10^{-4} eV and that for relaxation of the ionic degree of freedom to 1.36×10^{-3} eV. Our calculated bulk lattice constant of rutile RuO_2 was $a = 4.641$ Å and $c = 3.202$ Å, which are in reasonable agreement with experiment ($a = 4.51$ Å and $c = 3.11$ Å). Our values (6.56 Å by 3.20 Å) for RuO_2(1 1 0) surface compare favorably with experimental values of RuO_2(1 1 0) thin film (6.4 ± 0.3 Å by 3.1 ± 0.2 Å) grown on Ru(0 0 0 1) surface [2].

To simulate reaction process of the type A + B → C, we needed to include at least three Ru_{cus} sites in our surface unit cell. Therefore, we used a (3×1) surface unit cell of dimension 9.60×6.56 Å^2. The slab supercell consists of three O–RuO–O-layers of Ru and O atoms, separated by 18 Å of vacuum. NH_3 and other molecules were adsorbed on one side of the slab only. These molecules and substrate atoms in the first O–RuO–O-layer were fully relaxed, while the substrate atoms in the other layers were held fixed at their bulk-terminated positions.

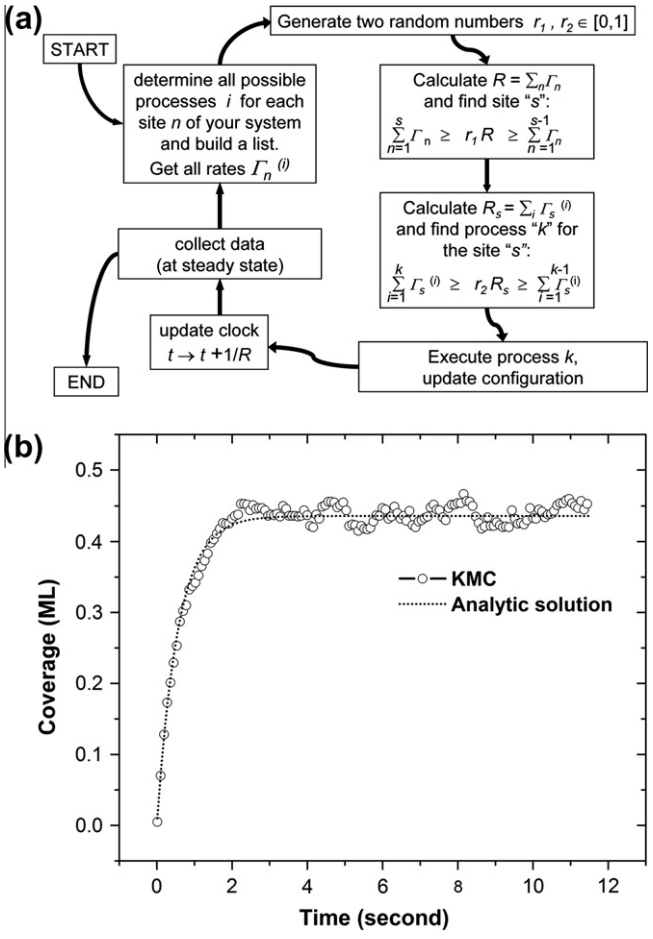

Fig. 3. (a) A standard KMC algorithm. (b) The transient solutions obtained by the KMC algorithm in (a) (circles) and by solving directly the differential equation $\frac{d\theta}{dt} = r_a(1-\theta) - r_d\theta$ (dots) for adsorption rate $r_a = 0.775129$ and desorption rate $r_d = 1.00301$ (event/site/s). The analytic solution corresponds to $\frac{r_a}{r_a+r_d}(1 - e^{-(r_a+r_d)t})$.

2.3. KMC algorithm

Fig. 3a shows the KMC algorithm [21,22] implemented in our code. For calculation of the reaction rate for a list of microscopic processes (some of which are shown in Fig. 2) we used: $\Gamma = \frac{sP}{\sigma\sqrt{2\pi mkT}}$ for adsorption process, where s, P, σ, m, k, and T are the sticking coefficient, partial pressure, site density, mass, Boltzmann constant, and temperature, respectively. For desorption and all other processes of interest, we used $\Gamma = \Omega_0 e^{-\frac{E_b}{kT}}$, where Ω_o is the preexponential (prefactor for short, also called trial frequency) and E_b is the energy barrier. The total reaction rate $R(k)$ in kth KMC run is the sum of total site rates $\Gamma_n(k)$ at each site n on the surface, which in turn is the sum of the individual process rate $\Gamma_n^{(i)}(k)$ of process i at site n in the kth KMC run: $R(k) = \sum_n^{\text{all-sites}} \Gamma_n(k) = \sum_n^{\text{total-sites}} (\sum_i^{\text{total-processes}} \Gamma_n(k))$. Site s is selected if $\Gamma_s(k)$ satisfies the condition $\sum_n^{s-1} \Gamma_n(k) < r_1 R(k) \leqslant \sum_n^{s} \Gamma_n(k)$ for a random number $0 < r_1 < 1$. Once a site is chosen, the selection of process is made in a similar manner by generating another random number r_2. Right after the execution of the selected process at the chosen site s, local scan is performed around the selected site in search of new processes. The total site rate $\Gamma_n(k)$ for those scanned sites and, accordingly, total reaction rate $R(k)$ are then updated. Finally, at the end of each iteration, the system clock is forwarded by an average time-step of $1/R$ $\left(\text{specifically. } t(k) \rightarrow t(k-1) + \frac{1}{R(k)}\right)$, with the result that simulation time is able to reflect physical time [23,24]. The above-mentioned procedures are cycled until the system reaches a steady state, at which point statistics are collected. In order to ascertain the randomness of generated numbers, the pseudorandom number generator is reset every 1 million steps.

To ensure the reliability of our KMC code, we have compared in Fig. 3b the attainment of saturation coverage for a simple system consisting of only two processes – adsorption and desorption. The KMC result follows closely the analytical solution, obtained from the differential equation $\frac{d\theta}{dt} = 0.775129(1-\theta) - 1.00301\theta$.

2.4. Calculation of activation energy barriers

For any reaction, the defining geometries are those of initial (IS), transition (TS), and final states (FS). Given IS and FS, we find the TS geometry by using the drag method, together with DFT structural relaxation algorithms. In the drag method, which is based on the assumption that forces on atoms vanish at the transition state, two reactant species are drawn toward each other step-by-step along the reaction coordinate in a controlled manner until the forces on each reactant become negligible. The negligible force configuration is equivalent to the configuration of single negative harmonic mode, which defines transition-state geometry. For example, when NH_3 decomposes into NH_2 on the RuO_2(1 1 0) surface by giving a hydrogen atom to nearby O_{cus} on the RuO_2(1 1 0)

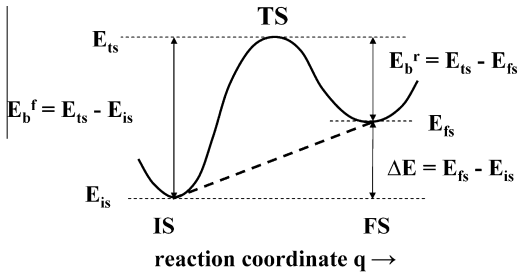

Fig. 4. KMC energy barriers. See description in text.

surface, the reaction coordinate is defined as the lateral displacement of the hydrogen atom dragged from the Ru_{cus} at the initial ammonia adsorption site. During dragging, the coordinate of the hydrogen atom along the reaction coordinate is fixed, while all other coordinates of the hydrogen atom and all coordinates of all other atoms are free to relax until the forces associated with those coordinates become negligible.

From the thus-calculated total energy of TS, we extract the activation energy (aka energy barrier) for the forward reaction ($E_b^f = E_{ts} - E_{is}$) and for the reverse reaction ($E_b^r = E_{ts} - E_{fs}$) as shown in Fig. 4. In several cases, we have also used the climbing-image, nudged elastic-band method (CI-NEB) [25] to calculate the energy barrier and found good agreement with the results from the drag method. For the spontaneous process ($E_b^f = 0$ & $\Delta E < 0$), we simply set the activation energy to zero, while for the reverse process of the spontaneous reaction we set the activation energy equal to the total energy change $\Delta E = E_{fs} - E_{is}$. For prefactors Ω, we used a standard value of 10^{13} s^{-1} for all processes in this study.

3. Results and discussion

3.1. Structure of $NH_{x(x=1-3)}$ on the RuO_2(1 1 0) surface

Table 2 presents our calculated binding energy for $NH_{x(x=1-3)}$ and other pertinent species on the RuO_2(1 1 0) surface along with results from previous studies [8,9]. Note that our calculated geometry and energy correspond to a 1/3 ML coverage; the coverages addressed by previous studies are indicated in Table 2.

We begin with single adsorption – as opposed to coadsorption – of NH_x species on RuO_2(1 1 0). The calculated adsorption energy of NH_{3cus} (1.46 and 1.55 eV with/without zero-point energy correction, respectively) is in good agreement with previous studies [8,9] and in reasonable agreement with experiment (1.25 eV at low coverage [1]). Our calculated adsorption energy for NH_{2cus} is smaller than that in Ref. [8], although the equilibrium geometry is in good agreement (Table 3). For NH on RuO_2(1 1 0), we find NH_{cus} to be unstable since it forms a bond with O_{br} strong enough to completely extract the hydrogen. This is possibly the easiest way to form N on RuO_2(1 1 0). As we shall see later, there is a competition between O_{br} and O_{cus} species for hydrogen bonding with $NH_{x,cus}$ species. The structural characteristics of RuO_2(1 1 0) as represented by the rows of O_{br} atoms and strong O adsorption on the reactive Ru_{cus} sites offer fundamental advantages for reactions that involve H abstraction, such as ammonia decomposition reactions.

We now turn to the coadsorption of NH_x with either O or OH on RuO_2(1 1 0). Both NH_x and either dissociated O_2 or intermediate OH adsorb on top of the Ru_{cus} sites. (For reasons that will emerge in our discussion of kinetics, adsorption of dissociated O_2 and OH_x species on top of O_{br} is not of primary interest for this study and thus not investigated.) Our calculated equilibrium structure for the coadsorption of NH_{2cus} and O_{cus} clearly shows that NH_{2cus} makes a strong bond with O_{cus}, with a bond length d(N–O) of 1.42 Å, much shorter than that found in a previous study [8]. Correspondingly, our calculated adsorption energy for this coadsorption (2.95 eV) is larger than that found in that study (2.45 eV; cf. Table 2). As for the coadsorption of NH_{cus} with O_{cus} and OH_{cus}, we found NH_{cus} to be unstable, as discussed earlier for the single adsorption of NH_{cus}: the hydrogen of NH_{cus} is immediately abstracted by O_{cus} (or by OH_{cus}) leaving the N atom at one Ru_{cus} site and the OH (or H_2O) at another Ru_{cus} site. It is noteworthy that this H abstraction does not occur spontaneously in the structural relaxations unless the hydrogen is pushed toward the O_{cus} or OH_{cus}, because of the flatness of the potential energy surface (PES) generated in the abstraction process at the Ru_{cus} site (where NH is adsorbed).

3.2. Reaction processes, their schematics and energetics

Fig. 2a gives an overview of various elementary processes (adsorption, desorption, decomposition, diffusion, and surface

Table 2
Adsorption energies (eV) of $NH_{x(x=1-3)}$ and other pertinent species on the RuO_2(1 1 0) surface at 1/3 ML coverage.

Species	Single adsorption		Coadsorption	
	This study	Wang et al.[b] (Ref. [8]) (except those listed)	This study	Wang et al.[b] (Ref. [8])
NH_{3cus}	1.55[a]	1.56 (1.55[c])	1.78 (O) 1.83 (OH)	1.71 (O) 1.86 (O)
NH_{2cus}	2.09	2.47	2.95 (O) 2.18 (OH)	2.45 (O)
NH_{cus}	Unstable	4.23	2.19 (H_2O)	4.29 (O)
NO_{cus}	1.76[d]	2.09	1.58 (O) 1.70 (N)	–
N_{2cus}	0.56	0.53	0.33 (O)	–
OH_{cus}	2.65	–	2.93 (NH_3)	–
H_2O_{cus}	1.09	1.22	–	–
N_{cus}	2.63	–	2.55 (OH) 2.58 (NO)	–
O_{cus}	3.54	–	3.55 (NH_3) 4.17 (NH_2) 3.36 (NO)	–

[a] Without zero-point energy correction (ZPEC). With ZPEC, 1.46 eV.
[b] For ½ ML coverage. DFT + VASP (Vienna *Ab initio* Simulation Package).
[c] Ref. [9]. DFT + VASP. Coverage is not reported.
[d] With ZPEC, 1.65 eV.

Table 3
Structural parameters (Å) for $NH_{x(x=2-3)}$ species on RuO_2(1 1 0) surface at 1/3 ML coverage.

	$d(N_{cus}–H_{cus})$		$d(N_{cus}–Ru_{cus})$		$d(N_{cus}–O_{cus})$[a]	
	This study	Wang et al. (Ref. [8])	This study	Wang et al. (Ref. [8])	This study	Wang et al. (Ref. [8])
NH_3	1.02	1.03	2.17	2.16	–	–
NH_2	1.02	1.03	1.95	1.93	1.42	≈3.0

[a] Upon the coadsorption with O_{cus}.

reactions) involving the intermediates considered in our simulations when the RuO_2(1 1 0) surface is exposed to NH_3 and O_2 gases. A possible scenario for the different stages in the ammonia decomposition process is depicted in Fig. 2b. Here, the ammonia decomposition process [steps (a) and (b)] is initiated with the introduction of surface on-top O species from dissociation of O_2 on the RuO_2(1 1 0) surface [denoted $O_{(s)}$]. This surface atomic oxygen takes two H atoms from ammonia and desorbs as a water molecule [step (a) in Fig. 2b]. The ammonia decomposition process alone requires an activation energy of 0.56 eV, while the desorption of the end product H_2O requires an energy of 1.09 eV. The final step of ammonia decomposition [step (b) in Fig. 2b] occurs through two channels. In one, atomic O is responsible, while in the other OH, one of the intermediate products of the precedent step (a) is responsible for the reaction with the NH from the same step. The reaction products so generated are atomic N and either OH or H_2O. As we shall see this exothermic NH decomposition reaction [step (b) in Fig. 2b] is a spontaneous, non-activated process. The thus-produced N atom combines in the subsequent reactions either with O [step (c) in Fig. 2b] deriving from the dissociation of an adsorbing O_2 molecule or with N [step (d) in Fig. 2b] that is a product of the ammonia decomposition taking place at a different Ru_{cus} site on the same RuO_2(1 1 0) surface. Step (c) requires an activation energy of 0.14 eV and leaves a NO molecule as the end product. This surface NO species has a high binding energy [8,9,26] and requires a high activation energy for desorption [step (e) in Fig. 2b]. The N_2-formation process [(d) in Fig. 2b] is in competition with the NO-formation process [(c) in Fig. 2b]; its activation energy, however, is twice that of the process yielding NO. The end product N_2 desorbs immediately at the high surface temperature (>500 K).

We present in Table 4 a complete list of reaction processes considered in our KMC simulations for ammonia decomposition on the RuO_2(1 1 0) surface, together with their respective prefactors and energy barriers. While in reality there may be more processes than those featured in Table 4, for the purpose of current KMC simulations we have found that this set provides a reasonable description of the reaction kinetics, with results in agreement with experiment.

We turn now to the discussion of the processes contained in Table 4. Since ammonia and oxygen are the only species controlled externally, their adsorption and desorption need to be accounted for in the simulations. P1 and P3 are such adsorption processes for NH_3 and O_2, respectively, while P2 and P4 are the desorption processes for NH_3 and O_2, respectively. The desorption energy barrier for NH_3 was set to the adsorption energy of NH_3 on RuO_2(1 1 0), 1.46 eV [1.55 eV without zero-point energy (ZPE) correction]. (cf. Table 2) Since O_2 dissociatively adsorbs on RuO_2(1 1 0) surface, its desorption barrier was set to the adsorption energy of atomic O_{cus}, 1.26 eV, which is the energy level of two O_{cus} atoms on the RuO_2(1 1 0) surface with respect to O_2 in gas phase.

The NH_3 decomposition reaction discussed earlier [step (a) in Fig. 2b], in fact, can itself be split into two steps: P5 and P6 in Table 4.

$$NH_{3cus} + O_{cus} \rightarrow NH_{2cus} + OH_{cus} \quad (P5)$$

$$NH_{2cus} + OH_{cus} \rightarrow NH_{cus} + H_2O \uparrow \quad (P6)$$

In step P5, NH_{3cus} reduces to NH_{2cus} via H abstraction by O_{cus}. This NH_{2cus} species subsequently decomposes via H abstraction by OH_{cus}, which itself was likewise formed in the precedent step P5, yielding as the end products NH and H_2O, the latter (H_2O) desorbing from the surface immediately at the high surface temperature (>500 K). (Note that H_2O_{cus} on RuO_2(1 1 0) completely desorbs below 450 K [1,9,27,28].) As shown in Fig. 5, the calculated forward and reverse energy barriers for P5 (E_b^f and E_b^r, respectively, in Fig. 3) are 0.55 and 0.26 eV, respectively, while E_b^f for the second step (P6) is 0.27 eV, in fair agreement with the previous DFT studies [8,9] where the values are slightly higher (cf. Table 5). If we suppose that P5 and P7 occur successively without interruption, the

Table 4
Reaction processes examined in this study. Vacancy and gaseous species are denoted as ∗ and g, respectively. {} indicates that the number inside is total energy change $\Delta E = E_{fs} - E_{is}$ instead of E_b.

	Reactants		Products		Prefactor (s^{-1})	E_b {or ΔE} (eV)
	A	B	C	D		
P1	∗	NH_3(g)	NH_3		1.0	0.0
P2	NH_3		∗	NH_3(g)	10^{13}	1.46
P3	2∗	O_2	O	O	1.0	0.0
P4	O	O	2∗	O_2	10^{13}	1.26
P5	NH_3	O	NH_2	OH	10^{13}	0.55
P6	NH_2	OH	NH	H_2O(g)	10^{13}	{0.27}
P7	NH	OH	N	H_2O(g)	10^{13}	0.0
P8	NH	O	N	OH	10^{13}	0.0
P9	N	O	NO	∗	10^{13}	0.14
P10	N	N	2∗	N_2(g)	10^{13}	0.27
P11	NO		∗	NO(g)	10^{13}	1.49
P12	N	∗	∗	N	10^{13}	0.96
P13	O	∗	∗	O	10^{13}	0.93
P14	OH	∗	∗	OH	10^{13}	1.12
P15	NH_2	O	NH	OH	10^{13}	{1.0}
P16	NH	OH	NH_2	O	10^{13}	0.0
P17	NH_2	OH	NH_3	O	10^{13}	0.26
P18	N	OH	NH	O	10^{13}	{0.9}

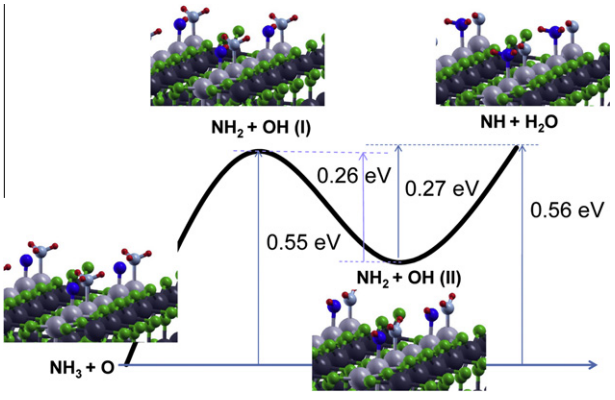

Fig. 5. PES for NH_3 decomposition, $NH_{3cus} + O_{cus} \rightarrow NH_{2cus} + OH_{cus}$ (I) → $NH_{2cus} + OH_{cus}$ (II) → $NH_{cus} + H_2O_{cus}$. Color coding: gray (Ru), green/blue (O), light blue (N), red (H). (For interpretation of the references to color in this figure legend, the reader is referred to the web version of this article.)

overall energy barrier would be still 0.56 eV (see Fig. 5), which corresponds to an activation temperature of 210 K, in good agreement with experiment (250 K) [1]. However, the first-stage activation energy for NH_3 decomposition (0.55 eV) alone is at odds with experiment (90 K) [1]. Interestingly, the total energy change (0.29 eV in Fig. 5) for the first-stage H abstraction corresponds to a reaction temperature of 110 K, which is close to experiment (90 K). However, this temperature (110 K) is obtained only when there is no activation energy for the reaction. We speculate, therefore, that there could be a non-activation reaction pathway for the first-stage H abstraction (P5) at the RuO_2(1 1 0) surface.

We turn now to the discussion of the possibility of the first H abstraction reaction of ammonia through O_{br} rather than O_{cus}. This reaction process can be written as follows:

$$NH_{3cus} + O_{br} \rightarrow NH_{2cus} + OH_{br} \quad \text{(P5a)}$$

The calculated energy barrier for this reaction (P5a) is 0.62 eV in close agreement with that of previous studies (0.44 [8]–0.67 [9] eV). (cf. Table 5) Thus, the activation energy of the first H abstraction reaction of ammonia via O_{br} (P5a) is as low as that of the H abstraction reaction via O_{cus} (P5). However, what makes the former (P5a) less probable than the latter (P5) is the flatness in the PES of the former. We present this PES in Fig. 6. There is hardly any valley at the final state. In fact, there is no distinction between TS and FS. (Note that such a flat PES was also reported in Ref. [8].) Therefore, this process (P5a) is kinetically unfavorable, since its reverse process – recombination of NH_{2cus} and H_{br} to form NH_{3cus} – will be exceedingly favored over the forward hydrogen abstraction process. In contrast, the PES of P5 (shown in Fig. 5) exhibits a potential well of 0.26–0.27 eV, which will enable P5 to proceed to the second hydrogen abstraction reaction process (P6) with a probability equal to that of the reverse process (P17 in Table 4). Thus, our DFT calculations clearly show that hydrogen abstraction reactions should occur through O_{cus} instead of O_{br}.

It is noteworthy that H abstraction energy decreases from 0.56 to 0 eV as the decomposition proceeds from P5 to P6, indicating that NH_{3cus} is the most stable while NH_{cus} is the most unstable [8,9]. In this regard, HREELS experiment shows an NH_{2cus}-related mode below 250 K [1]. Our DFT calculations also indicate that NH_{2cus} is possibly stable at low temperature, as it is locked by a potential well of 0.26–0.27 eV (cf. Fig. 5). However, NH_{2cus} is not observed in the core-level shift experiments [9]. The HREELS experiments also show that NH_{2cus}-related mode vanishes above 250 K [1]. These findings indicate that NH_{2cus} is unstable at high temperature. Indeed, our KMC simulations at 500–530 K show that NH_2 coverage is extremely low (<0.005 ML) at all pressure ranges investigated. This is because NH_{2cus} either converts to N_{cus} via H abstraction reaction with nearby OH_{cus} or recombines with nearby OH_{cus} to form NH_{3cus}. Thus, the potential well of 0.26–0.27 eV is not large enough to stabilize NH_{2cus} on RuO_2(1 1 0) surface.

It is illuminating to examine the structural changes from NH_{2cus} + OH_{cus} (I) to NH_{2cus} + OH_{cus} (II) (see Fig. 5 for details). This transformation involves two structural changes: (1) rotation of the H–N–H bond of NH_{2cus} by 90° around the N_{cus}–Ru_{cus} axis, so that the H–N–H bond points toward the OH_{cus}; (2) rotation of the O–H bond of OH_{cus} clockwise around the axis pinned on O_{cus}, so that O–H bond ends up aligned along the [1–10] direction. As a result of these changes, the total energy of NH_{2cus} + OH_{cus} (II) is lowered by 0.26 eV with respect to that of the pre-transformation geometry [NH_{2cus} + OH_{cus} (I)]. These two structural changes are driven by the formation of the hydrogen bond $H_{cus}\cdots O_{cus}$ between the hydrogen of NH_{2cus} and the oxygen of OH_{cus}. The shorter hydrogen bond length in NH_{2cus} + OH_{cus} (II) configuration (1.7 Å) than in NH_{2cus} + OH_{cus} (I) configuration (2.74 Å) indicates that the hydrogen bond $H\cdots O_{cus}$ in the NH_{2cus} + OH_{cus} (II) configuration is stronger than the hydrogen bonds $H\cdots O_{br}$ in the NH_{2cus} + OH_{cus} (I) configuration. Overall, this special case is a typical example of the crucial role of the hydrogen bonding between reactants in the ammonia decomposition reactions on the RuO_2(1 1 0) surface [8,9].

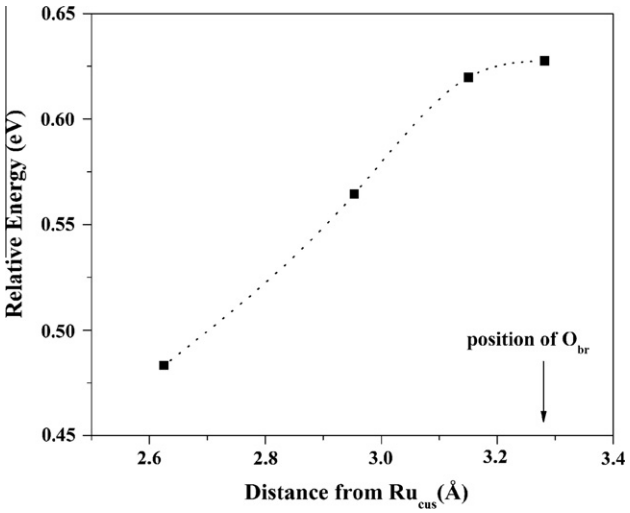

Fig. 6. PES for hydrogen abstraction reaction of NH_{3cus} by O_{br}.

In the final phase [(b) in Fig. 2b] of the ammonia decomposition process, NH_{cus} reacts either with OH_{cus} [P7 in Table 4] or with O_{cus} [P8 in Table 4]. These two reaction processes are among the fastest for ammonia decomposition on RuO_2(1 1 0) since they are non-activated. According to our calculations, the hydrogen of NH_{cus} can be easily abstracted by either O_{br} or cus-oxygen species (O_{cus} or OH_{cus}). However, this prediction seems to be at odds with a recent experiment reporting that O_{br} atoms are inactive during the reaction [1]. The inactivity of O_{br} may be the result of either a strong competition with O_{cus} for making stronger hydrogen bonding or of passive involvement of O_{br} atoms in hydrogen delivery reaction. In the former scenario, since $H\cdots O_{cus}$ is stronger than $H\cdots O_{br}$, hydrogen abstraction may occur via O_{cus} rather than via O_{br}, the latter thus remaining inactive, as shown earlier. In the

Table 5
Comparison of calculated energy barriers among recent DFT studies for some selected reaction processes. P5, P6, P9, and P10 denote the processes so designated in Table 4. QE (Quantum Espresso) and VASP (Vienna *Ab Initio* Simulation Package) indicate computer codes used in the studies, PBE and PW91 indicate GGA exchange–correlation functionals; and drag and NEB (Nudged Elastic Band) specify the methods for finding transition states (N/A: not reported in the study referenced).

Reaction process	This study (QE, PBE, drag)	DFT-GGA[a] (VASP, PW91, NEB)	DFT-GGA[b] (VASP, PBE, N/A)
P5	0.55	0.71	0.75
P6	0.27	0.31	0.30
P9	0.14	0.47	0.79
P10	0.27	0.20	N/A
Hydrogen abstraction of ammonia via O_{br}	0.62	0.44	0.67

[a] Ref. [8].
[b] Ref. [9].

latter scenario, O_{br} can simply take hydrogen atoms from some N-containing species on the $RuO_2(1\,1\,0)$ surface and deliver them to some other species, as in the hydrogen transfer reaction [29] found in water production on the $RuO_2(1\,1\,0)$ surface. In this case, O_{br} will remain passive at Ru_{bridge}.

Nevertheless, an active role of O_{br} in the catalytic ammonia oxidation reactions cannot theoretically be ruled out, since O_{br} can abstract hydrogen atoms from N-containing species and form water molecules, which can then move to Ru_{cus}, leaving an O_{br} vacancy at Ru_{bridge} [27]. Thus, O_{br} atoms can bring about O_{br} vacancies, which in turn can act as reactive sites for N-containing species at low O_2 pressure. In high O_2 pressure, O_{br} vacancies are expected to be filled immediately (either by dissociating O_2 species or by O_{cus}), since O_{br} has a much higher binding energy (4.6 eV [13]) than any other species ($NH_{x,cus}$ or O_{cus} or $OH_{x,cus}$) on the $RuO_2(1\,1\,0)$ surface. (Note that since our KMC lattice does not include O_{br} sites, our KMC simulations do not address this scenario.) However, the scenario described earlier in which N-containing species adsorb at a O_{br} vacancy probably not taking place, since no N-containing species adsorbed at O_{br} sites was detected in experiments [1,9]. Nonetheless, the hydrogen-bonding-initiated spontaneous decomposition reactions of NH by oxygen species on $RuO_2(1\,1\,0)$ point to the fundamental advantage of this surface for catalytic ammonia decomposition: by offering abundant O species both in the form of the 1D array of bridge-oxygens (O_{br}) and, from the dissociative adsorption of the O_2 molecule, in the form of cus-oxygens (O_{cus}), it fosters hydrogen abstraction from H-containing species.

P9 is a NO-recombination process with an activation energy of 0.14 eV [(c) in Fig. 2b], while P10 is a N_2-recombination and associative-desorption process with an activation energy of 0.27 eV [(d) in Fig. 2b]. The activation barrier for the recombination reaction (P9) of N_{cus} and O_{cus} to form NO_{cus} is fairly low. However, the HREELS showed that NO formed at as low as 250 K [1]. (A vibrational mode of 221 meV at 250 K and that of 226 meV at 320 K were associated with N–O stretching mode.) The core-level shift spectroscopy also showed a NO peak at and above 350 K (although even a weak feature at 300 K and a very weak feature at 250 K are possibly associated with NO peak) [9]. In fact, according to our KMC simulations, the peak reactivity of the decomposition reaction of NH_{3cus} to N_{cus} occurs at 210 K with the activation energy of 0.56 eV. Thus, the reported NO-formation temperature in the HREELS experiment [1] (250 K) corresponds approximately to the temperature at which the decomposition reaction occurs. Therefore, it is clear that NO-formation is not controlled by the NO-formation barrier of 0.14 eV, but rather by the energy barrier (0.56 eV) of its precedent processes, i.e., the NH_3 oxidation reactions (P5–P6 in Table 4).

P11 [(e) in Fig. 2b] is a NO-desorption process, while P12–P14 are diffusion processes. Inclusion of these diffusion processes in our study is necessary since they play a significant role in increasing reaction rates and thereby in selectivity. Although P16 – a reaction of NH_{cus} and OH_{cus} to produce NH_{2cus} and O_{cus} – works to inhibit ammonia decomposition overall, its reverse, P15, while energetically less favorable, is likely to increase as O_2 pressure increases upon the surface. Finally, P17 and P18 are the reverse processes of P5 and P8, respectively. The reverse processes for P6 and P7 are not included in our KMC simulations because one of the end products is vapor (H_2O), which desorbs immediately owing to a high surface temperature (>500 K). Note that ZPE correction is not included in the energy barriers in Table 4 except for the energy barriers of P2 and P11.

Finally, we would like to note that there exists a non-trivial disagreement among recent DFT-GGA calculations [8,9] regarding the energy barrier of some of the catalytic reaction processes of ammonia oxidation on $RuO_2(1\,1\,0)$ surface. We present in Table 5 a comparison of our energy barriers calculated by the drag method with values from the previous theories employing other methods for calculation of energy barriers. For the hydrogen abstraction process of ammonia on $RuO_2(1\,1\,0)$ surface, our values are in reasonable agreement (within 0.14–0.2 eV) with those derived from other theories. Also, our value for the N + N recombination process is in good agreement with that of a previous study. However, when it comes to the energy barrier of the N + O recombination process, our energy barrier is substantially smaller than those of other studies (>0.3 eV). In fact, even the two DFT-GGA studies using the same code (VASP) but using different exchange–correlation functionals report substantially different energy barriers for this reaction process (>0.3 eV). So the accurate calculation of the activation energy of NO-formation process remains an outstanding issue. (The geometry of our transition state for N + O recombination process is available elsewhere [26].) However, as we shall discuss later, the decisive factor for selectivity of the $RuO_2(1\,1\,0)$ surface toward NO is not the energy barrier of N + O recombination process, but the relative probability of N_{cus} to meet O_{cus}.

3.3. Rate-limiting processes

The two directly pertinent experimental studies [1,9] point to H_2O_{cus} and NO_{cus} as rate-limiting species at low temperature. Particularly, the formation rate of NO_{cus} was greatly increased at a temperature of ~500 K, at which NO_{cus} desorbs according to TDS (thermal desorption spectroscopy). Theoretically, NO has a large binding energy on the RuO_2 surface (1.98 eV [9] and 1.49–1.65 eV [26] depending on NO coverage). When we employed 1.65 eV as the NO-desorption barrier in the KMC simulations at temperatures of 500–530 K, the resultant NO-formation rate was smaller than that of experiment by an order of magnitude. This was because in those calculations NO species remained at the surface, occupying ~30% of the Ru_{cus} sites. When we increased the NO-formation rate by reducing the NO-desorption barrier from 1.65 eV to 1.49 eV (scaling up the desorption rate by a factor of 13), NO blocking decreased to ~17% of the Ru_{cus} sites. The resulting NO-formation rate turned out to be comparable to that of experiment. Note that temperature was held constant throughout the simulation: the reaction rate increase resulted *solely* from reducing the desorption barrier. Alternatively, if we keep the NO-desorption barrier at 1.65 eV and instead increase the simulation temperature to 590 K (from 530 K), we *also* obtain a NO-formation rate comparable to experiment. The inference is clear that NO remaining on the surface inhibits all Ru_{cus}-mediated reactions by blocking Ru_{cus} sites.

Another process that has a global impact on the formation rates of NO and N_2 turns out to be N diffusion (P12 in Table 4), which in turn is affected by two factors. For one, the diffusion barriers for N_{cus} and O_{cus} (0.93–0.96 eV) are relatively larger than the NH_3 decomposition barrier (0.56 eV). For another, N diffusion rate is directly connected to N availability at the surface, since N_{cus} is required for formation of both NO and N_2 and is generated only by NH_3 decomposition reactions. The recombination probability of both NO and N_2 is thus significantly reduced by intermediates that block potential diffusion sites.

3.4. KMC simulations of 18 processes

In the KMC simulations of our 18 processes, as in experiment, NH_3 pressure was fixed to 10^{-7} mbar for the entire O_2 pressure range, and O_2 pressure was varied from 0.5×10^{-7} to 20×10^{-7} mbar. Here, lattice points represent Ru_{cus} sites and the 1D nature of the $RuO_2(1\,1\,0)$ surface is simulated by setting the number of nearest neighbors for the lattice to 2 – left or right in a row – so that only reactants belonging to the same row can react with each other.

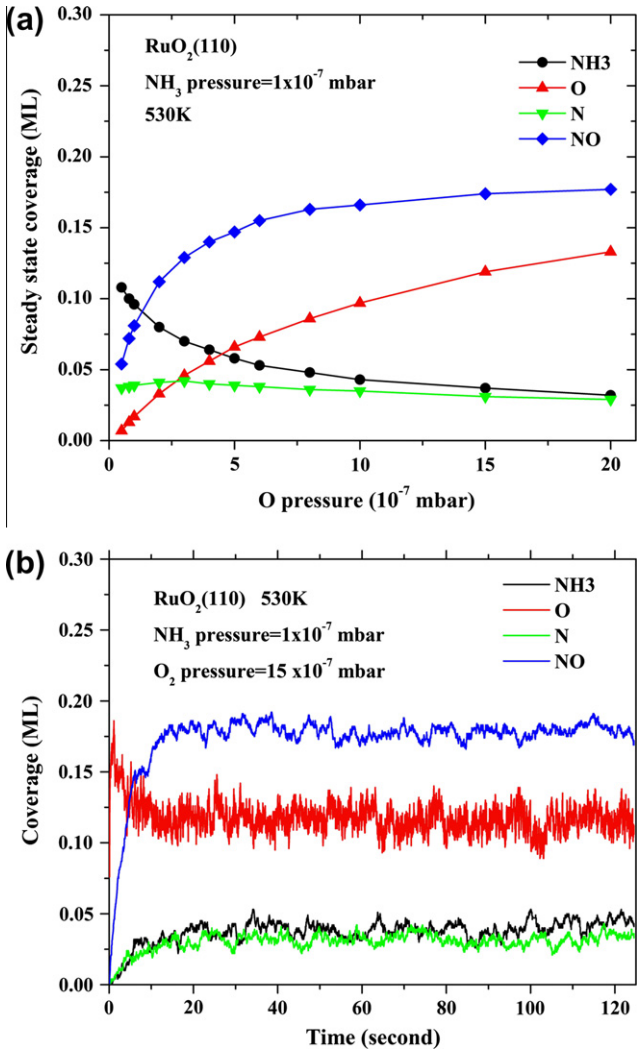

Fig. 7. (a) Steady-state surface coverage of selected species versus O pressure and (b) evolution of surface coverage versus reaction time for O_2 pressure of 15×10^{-7} mbar and NH_3 pressure of 10^{-7} mbar.

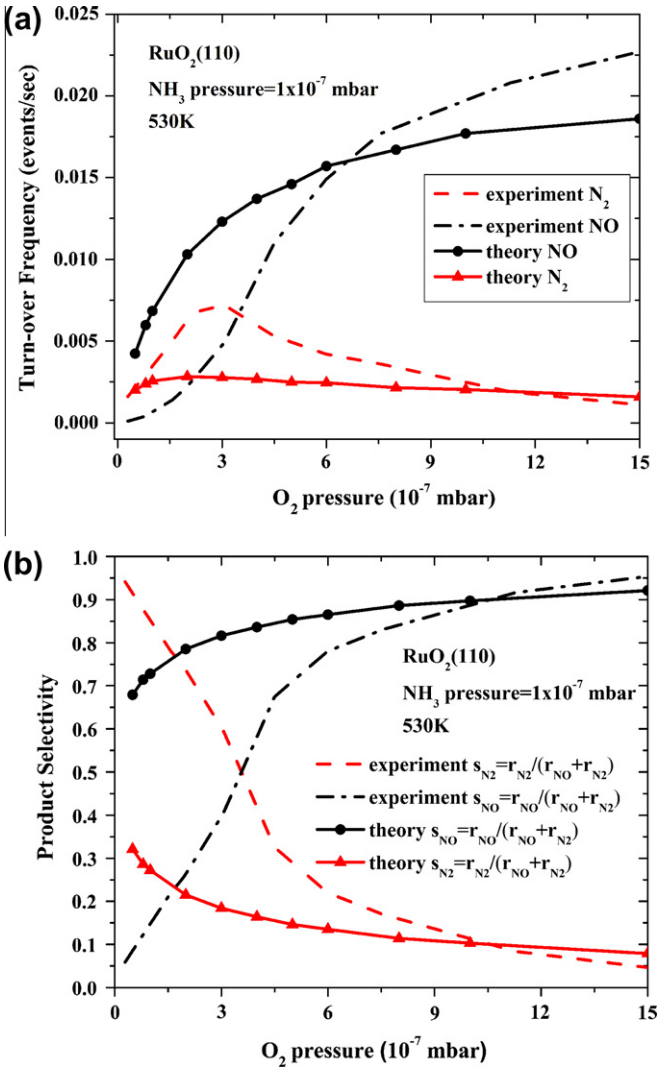

Fig. 8. Calculated reaction rates and selectivity at 530 K for NO- and N_2-processes in Table 4: (a) reaction rate (ML/s) and (b) selectivity. Dashed curves show experimental results from Ref. [1].

The binding energies of NH_{3cus} and NO_{cus} at RuO_2(1 1 0) surface exhibit a strong coverage dependence. For example (according to our calculations), NH_3 binding energy varies by 0.34 eV and that of NO by 0.16 eV. Consideration of coverage dependence of interactions is important in KMC simulations since it can significantly change the rates of adsorbate desorption. In our code, this coverage dependence is described by the multiplying factor $\exp(\varepsilon\theta/RT)$ of Γ [22], where ε is the repulsive interaction energy and θ is the coverage of adsorbate at the surface ($0 \leqslant \theta \leqslant 1$). To take into account this coverage dependence of the binding energies of NH_{3cus} and NO_{cus} in KMC simulations, we set ε to 0.34 eV for NH_{3cus} and 0.16 eV for NO_{cus}. We present our results for steady-state surface coverages with respect to O_2 pressure in Fig. 7a, those for the evolution of surface coverage versus the KMC time for an O_2 pressure of 1.5×10^{-6} mbar in Fig. 7b, and those for steady-state turn-over frequencies (TOF) with respect to O_2 pressure in Figs. 8 and 9. Data for steady-state statistics were sampled every 10^5 KMC step and each point in Figs. 7a, 8 and 9 represent a simulation of 2 billion steps – equivalent, on average, to a KMC time of about 140 s.

Fig. 7a clearly shows that at low O_2 pressure O and NO coverages increase proportionally to O_2 pressure while those of NH_3 and (in a weak sense) N decrease. At high O_2 pressure (>1.5×10^{-6} mbar), NH_3 coverage is almost equal to that of N, indicating that NH_3 effectively converts to N in the O-rich conditions. However, at low O_2 pressure (<10^{-7} mbar), only a fraction of NH_3 coverage converts to N, indicating that the NH_3 and NH decomposition processes (P5 and P8 in Table 4) are significantly restricted in such O-poor conditions.

Next, we turn to the calculation of product selectivity, which is defined in terms of NO and N_2-formation rates (or turn-over-frequencies) $\mathbf{r}_{NO}$ and $\mathbf{r}_{N2}$ as follows:

$$\mathbf{S}_{NO} = \frac{\mathbf{r}_{NO}}{\mathbf{r}_{NO} + \mathbf{r}_{N_2}} \quad (1)$$

$$\mathbf{S}_{N_2} = \frac{\mathbf{r}_{N_2}}{\mathbf{r}_{NO} + \mathbf{r}_{N_2}} \quad (2)$$

Fig. 8 shows the calculated reaction rates and selectivity for NH_3 decomposition on the RuO_2(1 1 0) surface for 530 K. (We omit results for 500 K since they are qualitatively quite similar to those for 530 K.) The reaction rates and selectivity toward NO show excellent agreement with experiment for O-rich conditions (>6×10^{-6} mbar). In particular, the predicted selectivity of 93% is in good agreement with experiment (~95%), corroborating the experimental results. However, for O-poor conditions (<5×10^{-7} mbar), the results of our

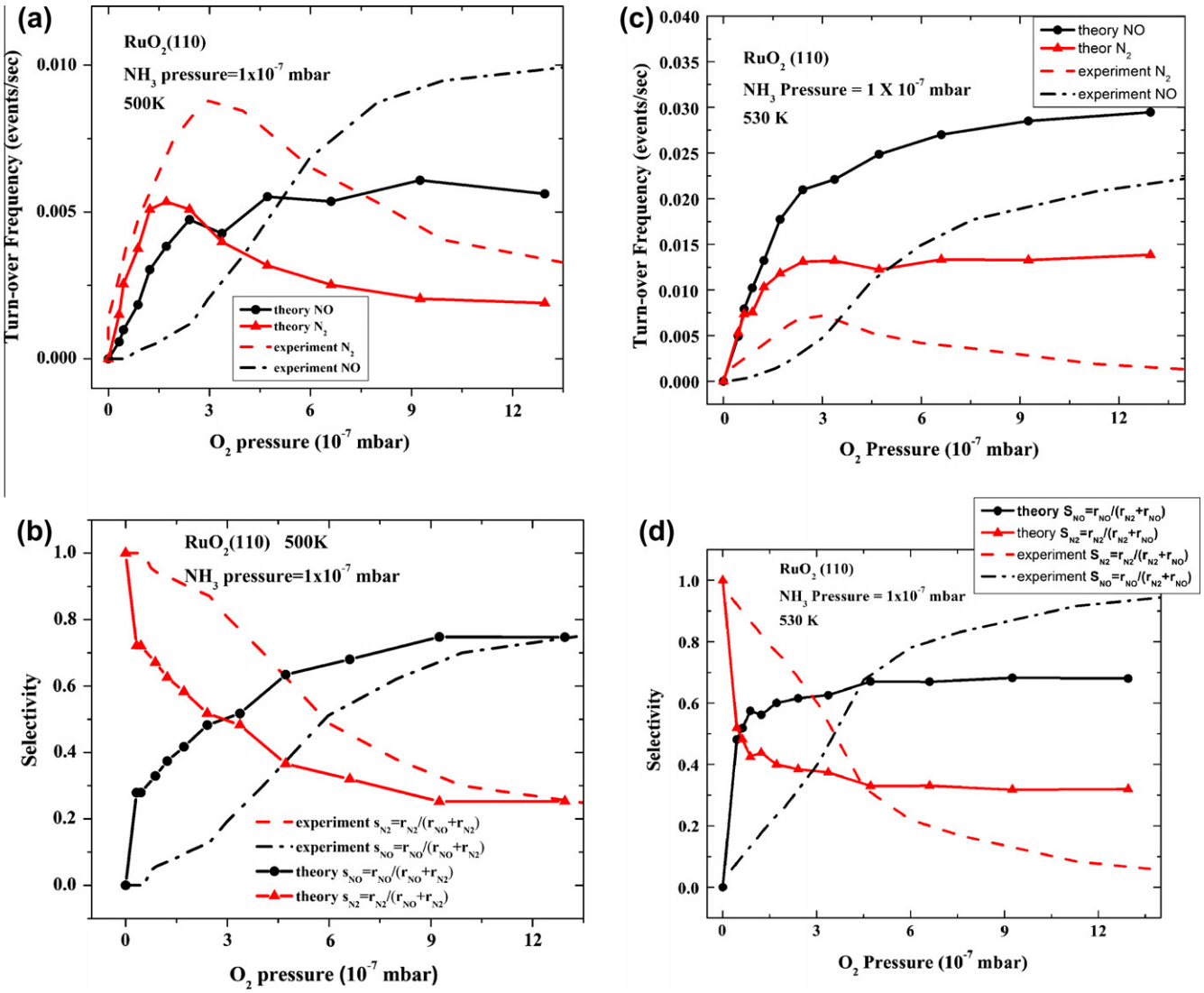

Fig. 9. Calculated reaction rates and selectivity for NO- and N_2-formation with a modified N diffusion barrier (0.76 eV) at (a)–(b) 500 K and (c)–(d) 530 K.

simulations based on the 18 processes in Table 4 are at odds with experiment in respect of both reactivity and selectivity: (1) our calculations overestimate the NO-formation rate and underestimate the N_2-formation rate; (2) they do not reproduce the crossover that occurs in experiment at an O_2 pressure of around 3×10^{-7} mbar.

To explain whether these discrepancies could be overcome by rethinking relevant diffusion barriers, we increased the N diffusion rate by changing the diffusion barrier from 0.96 eV to 0.76 eV. The results for 500 K and 530 K are presented in Fig. 9. The resulting increase in N diffusion did indeed significantly enhance not only the N_2 reaction rate but also, for 500 K, reproduced a crossover similar to that in experiment! Moreover, the resulting N_2 reaction rate at 500 K (Fig. 9a) and, less emphatically, the resulting NO and N_2 reaction rates at 530 K (Fig. 9c) exhibit trends similar to those of experiment, although their absolute values are less than one-half of those of experiment. But this adjustment fares no better in reproducing the findings of experiment overall, since at higher O_2 pressure it results in an NO reaction rate 57% higher than that entailed by our original diffusion barrier (compare Fig. 9c with Fig. 8a). This is so because faster N diffusion increases the probability of N + O combination at high pressures. Nevertheless, the fact that the rate of N + N combination substantially varies directly with the rate of N diffusion (compare Figs. 9c and 8a) means that N diffusion is a rate-limiting process for N_2-formation. This is particularly true at low O_2 pressure since at high O_2 pressure N blocking is more important.

3.5. Processes at low pressures

The above results suggest that surface diffusion is the only channel open to N + N recombination, while an additional channel is available for N + O recombination, namely NO_{cus} formation, the recombination of N_{cus} and O_{cus}, the latter formed by adsorption from O_2 dissociation induced by the proximity of already formed N_{cus} to an empty Ru_{cus} site. As a result, it is natural that the probability of N_{cus} to meet another N_{cus} is greatly reduced by the hindrance to N diffusion caused by such intermediate species as NH_x and OH_x. This explains why NO-recombination is always superior to that of N_2 in our KMC simulations (Fig. 8).

We have seen that it is not possible to generate results consistent with experiment by modifying N diffusion because N diffusion has a global effect for all O_2 pressures. In order to obtain good agreement with experiment for the whole pressure range, we need to include a process with a local effect, that is, a process that

enhances N_2 reaction rate (and suppresses NO reaction rate) in low O_2 pressure range alone. A clue may lie in the fact that in the experimental reaction rate curve of NO (Fig. 8), there is a change in reaction kinetics, namely, a curvature change from the positive to the negative curvature near the crossover pressure ($\sim 2 \times 10^{-7}$ mbar), at which N_2-formation rate also drops suddenly. While below the crossover pressure, NO-formation is significantly suppressed, above that pressure it starts to increase exponentially. The N_2 rate behaves in exactly opposite manner. This may be an indication that one (or more) process active only at low pressure enhances the N_2 rate and suppresses the NO rate. We speculate that such processes could involve bridge oxygen species [28], which are not included in our KMC simulations or defects (including steps) that may be present at the surface [26].

3.6. Factors in the high selectivity of NO over N_2

It may appear from the results of KMC calculations described so far (Figs. 8 and 9) that how NO-formation is selected is because its activation energy (0.14 eV) is smaller than that of N_2 (0.27 eV). However, the high selectivity of NO over N_2 is not a consequence of the difference in the activation energies of the two recombination processes, but lies in something more fundamental. This can be shown by KMC simulations employing the three end processes only: P9, P10, and P11 in Table 4 (holding the rates of N and O diffusion processes equal). The purpose of undertaking these simple model simulations is to highlight the importance of these processes which in essence provide an almost complete explanation of the experimental results. We begin by populating the lattice randomly with N and O atoms, varying the O coverage [O] from 0.1 to 0.5 ML while keeping [N] + [O] = 1 ML. (Hence, for example, at 0.5 ML coverage, the lattice is overlain with equal numbers of N and O atoms.) We allow the simulations to proceed until no executable processes remained. The statistics collected at the end of the simulations are the total number of NO and N_2 produced, from which we derive the formation rates for the two products.

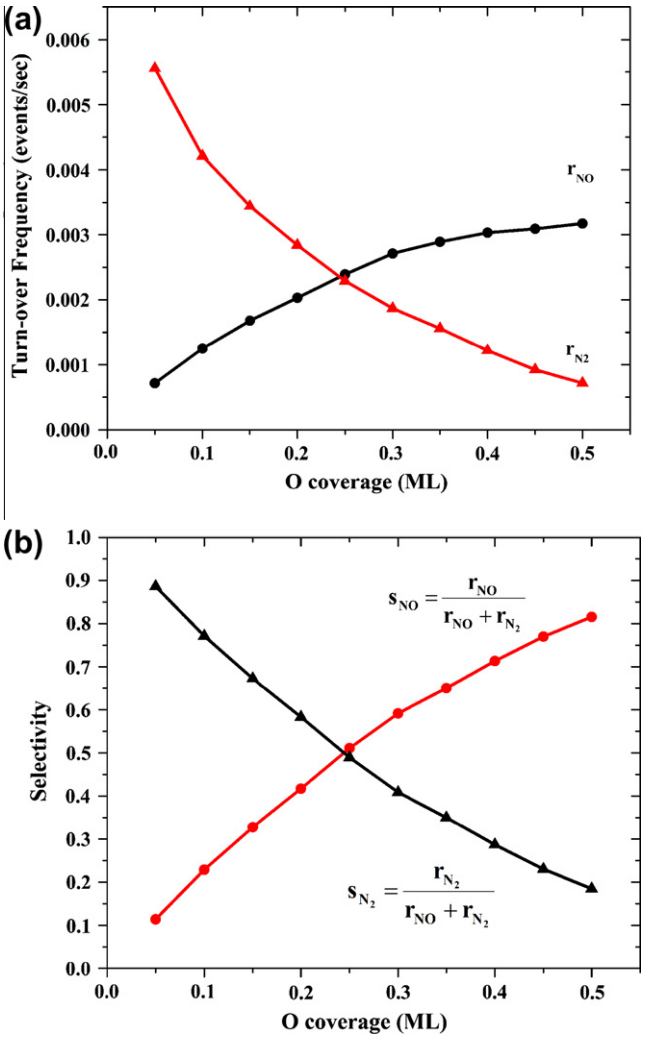

Fig. 10. KMC simulations of three end processes: (a) reaction rate and (b) selectivity plotted over initial O coverage.

The results presented in Fig. 10 show that with the three end processes only, a high selectivity of 81% was obtained for NO (Fig. 10b). Furthermore, the predicted reaction rates also clearly show a crossover as O coverage increases, in conformity with experiment (Fig. 10a). (Comparison of the absolute magnitudes of the resultant reaction rates with those of experiment is not meaningful since these simulation results are not steady-state quantities [there was no continuous flow of N and O atoms].) These results clearly indicate that the processes left out in these simple simulations – for example, the various ammonia decomposition processes [(a) and (b) in Fig. 2b; P5-P8 in Table 4] – are not responsible for the high *selectivity* of the $RuO_2(1\,1\,0)$ surface. They affect only the NO and N_2-formation rates, but not the divergence between them.

To pinpoint the effect on selectivity of the difference in the activation energy for the two competing NO and N_2-recombination processes [P9 and P10 in Table 4, respectively], we set the two energy barriers equal, specifically, to 0.14 eV in order to endow P9 and P10 with the same reaction rate.) The selectivity in favor of NO indeed reduced (from 81%) to 70%. Thus, the difference in the energy barriers of the two competing recombination processes has a significant effect on the selectivity. However, as we can see the selectivity is *still* maintained at 70%. (Note that diffusion of N or O in these simple simulations of three processes is not inhibited at all. That is, N will always meet either N or O. As a result, the probability of N to meet another N is much larger than that in realistic situations where N diffusion is severely inhibited. Therefore, N_2-formation rate in the simple simulations must be much larger than that in the realistic simulations of 18 processes.) Thus, the difference in the activation energies is not the reason for the high selectivity (81% for NO).

As Fig. 10 makes clear, even under N-dominant surface conditions ([N] ≫ [O]) the turn-over frequency of NO is still comparable to that of N_2, and the crossover occurs at an N coverage three times as large as the corresponding O coverage ([N] = 0.75 and [O] = 0.25). In fact, even at equal N and O coverages ([N] = [O] = 0.5ML), the probability of NO-recombination tends to be much higher than that of N_2-recombination. For NO-recombination, one N needs to sit next to an O atom, while for N_2-recombination two N atoms need to sit side-by-side. Let us imagine, for example, twenty random combinations of three N and three O atoms, in each of which those six atoms are set along a line. If we count all possible N + N and N + O combinations, N + O occurs three times more frequently than N + N. In principle, NO-recombination probability has linear dependence, while N_2-recombination probability has a quadratic dependence on the N coverage. This fundamentally different dependence of recombination probabilities of the two competing processes upon N coverage makes a marked difference in the reactivity and selectivity issues being examined here. Moreover, N availability is strongly reduced by a slow rate of N diffusion (via N blocking), while O availability is far less affected by O diffusion rate (via O blocking) owing to the nearby availability of O from dissociation of O_2. In this case, O_2 pressure, a measure of O_2 availability on the surface, can emerge as the controlling

parameter for the comparative reactivity and hence selectivity of the RuO_2(1 1 0) surface for NO.

4. Conclusions and summary

We have used a combination of density functional theory (DFT) and kinetic Monte Carlo (KMC) simulations to calculate the reaction rates for the selective oxidation of ammonia on RuO_2(1 1 0). We find that the overall energy barrier for $NH_3 + O \rightarrow NH + H_2O$ is 0.56 eV, while that for $N + N \rightarrow N_2$, and $N + O \rightarrow NO$ to be 0.27, and 0.14 eV, respectively. We find several factors contributing to the high reactivity of the RuO_2(1 1 0) surface toward catalytic ammonia decomposition: (1) dissociative adsorption of O_2; (2) an abundance of O species at the surface in the form of O_{br} or O_{cus} species; (3) H bonding between ammonia and its intermediates with the adsorbate and substrate O. Hydrogen bonding converts NH decomposition into a non-activated (spontaneous) process. However, the reactivity of the RuO_2(1 1 0) surface is severely limited by a large desorption barrier of NO since, at slow NO-desorption rate, most reaction sites (Ru_{cus}) are blocked by surface NO. Thus, to obtain high reactivity, a high temperature ($\sim$530 K) is needed. On the other hand, the formation rates of both NO and N_2 are depressed by slow N and O diffusion, both of whose barriers (0.96 eV and 0.93 eV, respectively) are relatively larger than the decomposition barrier (0.56 eV) of NH_3. And N and O diffusion are both in turn obstructed by various intermediates present on the RuO_2(1 1 0) surface. But slow N diffusion inhibits the recombination rate for $N + N \rightarrow N_2$ far more severely than it does the recombination rate for $N + O \rightarrow NO$, because the NO-formation process depends far less on N availability than does that for N_2-formation. This differential dependence on N coverage comes crucially into play when N availability is strongly limited by slow N diffusion (via N blocking). O availability, however, is not analogously limited by substrate conditions. Rather, O_2 pressure, a measure of the availability of O_2 at the surface, turns out to be the key controlling parameter for the selectivity of the RuO_2(1 1 0) surface in favor of NO. In summary, we find the decisive factor for the selectivity of the RuO_2(1 1 0) surface to be the differential nearby availability of N and O, resulting from slow N diffusion and steady dissociation of O_2, which amplifies the difference in the dependence on N availability of the recombination probabilities for the competing end processes.

Acknowledgment

The work is supported by DOE under Grant No. DE-FG02-aa07ER15842. We acknowledge fruitful discussions with S. Stolbov. We are grateful to Lyman Baker for careful reading of the manuscript and constructive comments.

References

[1] Y. Wang, K. Jacobi, W.-D. Schoene, G. Ertl, J. Phys. Chem. B 109 (2005) 7883.
[2] H. Over, Y.D. Kim, A.P. Seitsonen, S. Wendt, E. Lundgren, M. Schmid, P. Varga, A. Morgante, G. Ertl, Science 287 (2000) 1474.
[3] Y.D. Kim, H. Over, G. Krabbes, G. Ertl, Top. Catal. 14 (2001) 95.
[4] C.Y. Fan, J. Wang, K. Jacobi, G. Ertl, J. Chem. Phys. 114 (2001) 10058.
[5] J. Wang, C.Y. Fan, K. Jacobi, G. Ertl, Surf. Sci. 481 (2001) 113.
[6] N. López, J. Gómez-Segura, R.P. Marín, Pérez-Ramírez, J. Catal. 255 (2008) 39.
[7] J. Wang, C.Y. Fan, K. Jacobi, G. Ertl, J. Phys. Chem. B 106 (2002) 3422.
[8] C.C. Wang, Y.J. Yang, J.C. Jiang, J. Phys. Chem. C 113 (2009) 2816; C.C. Wang, Y.J. Yang, J.C. Jiang, D.S. Tsai, H.M. Hsieh, J. Phys. Chem. C 113 (2009) 17411.
[9] A.P. Seitsonen, D. Crihan, M. Knapp, A. Resta, E. Lundgren, J.N. Andersen, H. Over, Surf. Sci. 603 (2009) L113.
[10] M. Rössler, S. Günther, J. Wintterlin, J. Phys. Chem. C 111 (2007) 2242.
[11] K. Reuter, D. Frenkel, M. Scheffler, Phys. Rev. Lett. (2004) 116105; K. Reuter, M. Scheffler, Phys. Rev. B 73 (2006) 045433.
[12] S. Hong, A. Karim, S. Stolbov, T. Rahman, American Physical Society, 2009. APS March Meeting, March 16–20, 2009, abstract #T12.004. <http://meeting.aps.org/Meeting/MAR09/Event/98096>.
[13] Y.D. Kim, A.P. Seitsonen, S. Wendt, J. Wang, C. Fan, K. Jacobi, H. Over, G. Ertl, J. Phys. Chem. B 105 (2001) 3752.
[14] W. Kohn, L. Sham, J. Phys. Rev. 140 (1965) A1133.
[15] D. Vanderbilt, Phys. Rev. B 41 (1990) 7892.
[16] Our pseudopotentials are available from <http://www.pwscf.org/pseudo.php>. The name of the pseudopotential files used are Ru.pbe-n-van.UPF, O.pbe-van_ak.UPF, N.pbe-van_ak.UPF, and H.pbe-van_ak.UPF for Ru, O, N, and H, respectively.
[17] J.P. Perdew, K. Burke, M. Ernzerhof, Phys. Rev. Lett. 77 (1996) 3865.
[18] P. Giannozzi et al., J. Phys. Condens. Matter 21 (2009) 395502.
[19] H.J. Monkhorst, J.D. Pack, Phys. Rev. B 13 (1976) 5188.
[20] M. Methfessel, A. Paxton, Phys. Rev. B 40 (1989) 3616.
[21] J.S. Reese, S. Raimondeau, D.G. Vlachosy, J. Comput. Phys. 173 (2001) 302.
[22] S. Raimondeau, P. Aghalayam, A.B. Mhadeshwar, D.G. Vlachos, Ind. Eng. Chem. Res. 42 (2003) 1174.
[23] A.B. Bortz, M.H. Kalos, J.L. Lebowitz, J. Comput. Phys. 17 (1975) 10.
[24] K.A. Fichthorn, W.H. Weinberg, J. Chem. Phys. 95 (1991) 1090.
[25] G. Henkelman, B.P. Uberuaga, H. Jónsson, J. Chem. Phys. 113 (2000) 9901.
[26] S. Hong, T.S. Rahman, K. Jacobi, G. Ertl, J. Phys. Chem. C 111 (2007) 12361.
[27] M. Knapp, D. Crihan, A.P. Seitsonen, A. Resta, E. Lundgren, J.N. Andersen, M. Schmid, P. Varga, H. Over, J. Phys. Chem. B 110 (2006) 14007.
[28] A. Lobo, H. Conrad, Surf. Sci. 523 (2003) 279.
[29] M. Knapp, D. Crihan, A.P. Seitsonen, H. Over, J. Am. Chem. Soc. 127 (2005) 3236.